# IX. PHYSICAL ELECTRONICS AND SURFACE PHYSICS*


Academic and Research Staff

Prof. R. E. Stickney
Dr. M. L. Shaw

Graduate Students

F. W. Eberle
D. L. Fehrs
J. W. Gadzuk
W. Greaves
H. C. Juvkam-Wold
D. S. Shupe
S. Yamamoto


## A. DESORPTION, DISSOCIATION, AND RECOMBINATION OF HALOGEN GASES ON METAL SURFACES

### 1. Introduction

The purpose of this report is to describe our preliminary plans for an experimental study of the dissociation, recombination, and desorption of halogen gases on various metal surfaces. The desorption energy $E_d$ may be determined from measurements of the adsorption lifetime $\tau$, for various temperatures, based on the usual assumption that the relation between $\tau$ and $E_d$ can be expressed as

$$\tau = \tau_o \exp(E_d/kT). \tag{1}$$

The quantity $\tau_o$ is of the order of a lattice vibration period, that is, $\sim 10^{-12}$ sec. (Steiner and Gyftopoulos[1] have recently reported theoretical estimates of the desorption energies of halogen atoms on (110) tungsten, the values being 4.49 eV for F, 3.53 eV for Cl, 2.94 eV for Br, and 2.45 eV for I.) Equation 1 is plotted in Fig. IX-1 for $\tau_o = 1 \times 10^{-12}$ sec and several values of $E_d$. It can be seen that the temperature range corresponding to $10^{-4}$ sec $\leq \tau \leq 1$ sec is easily attainable.

The reasons for choosing the halogens follow.

(i) Because of their low dissociation energies, both atomic and molecular beams of halogens are easily obtained.

(ii) The halogens form a series of similar valence in the Periodic Table, and therefore allow comparison of parameters, such as ionization potential and dissociation energy, to correlate data.

(iii) Halogens would be convenient in a future study of surface catalysis with alkali atoms.


*This work was supported by the National Aeronautics and Space Administration (Grant NGR-22-009-091), the M.I.T. Cabot Solar Energy Fund, and the Joint Services Electronics Programs (U.S. Army, U. S. Navy, and U. S. Air Force) under Contract DA 28-043-AMC-02536(E).

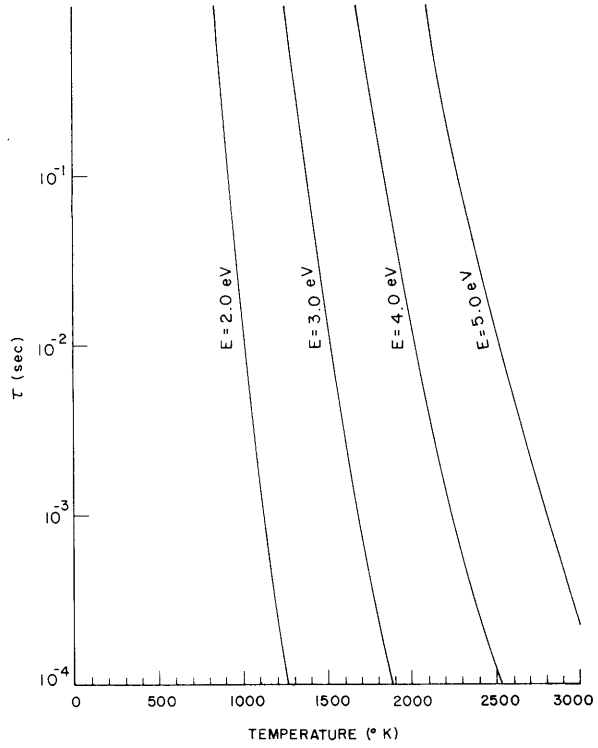


Fig. IX-1. Adsorption lifetime vs temperature.

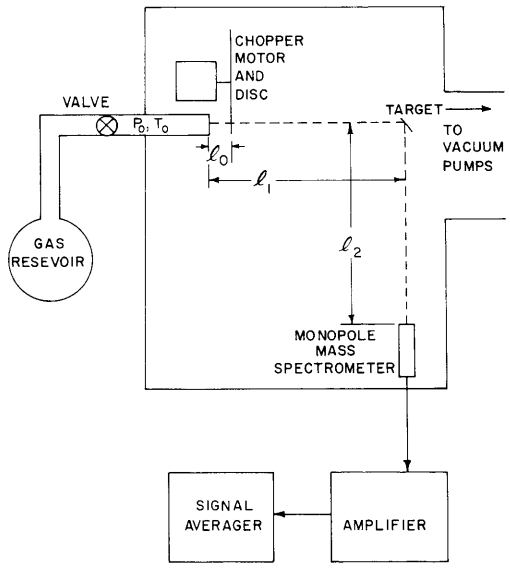


Fig. IX-2. Schematic diagram of test apparatus.

2. Apparatus

The experimental apparatus is shown in schematic form in Fig. IX-2. A metal ribbon target is resistance-heated to the desired temperature in a vacuum chamber, while a molecular beam of halogen gas is chopped by a rotating slotted disc and directed onto the target. The desorbed molecules from the target are detected by a monopole mass spectrometer. The desorbed beam signal is periodic in time, and after being amplified, is measured by a signal averager to separate the signal from the noise. The shape of the measured signal pulse contains information on the desorption time from which the desorption energy is determined.

3. Analytical Considerations

a. Beam Magnitude

The output signal of the mass spectrometer is directly proportional to the molecular density of the scattered beam. Hence, it is advantageous to design the apparatus so that this density is as large as possible. The limitations imposed by the pumping speed, chamber pressure, and system dimensions are considered here.

A molecular beam is produced by a gas at pressure $P_o = n_o kT_o$ effusing through a hole of area $A_o$ into the vacuum chamber. The molecular flux[2] entering the chamber, $\dot{N}_o$, is

$$\dot{N}_o = \frac{1}{4} A_o n_o \bar{v}_o \ \text{sec}^{-1}, \tag{2}$$

where $\bar{v}_o = (8kT_o/\pi m)^{1/2}$. In the design shown in Fig. IX-2, the beam is intercepted by a target of area $A_1$ at a distance $\ell_1$ from the beam source. If $\beta_1$ is the angle between the source normal and the target normal, then the molecular flux striking the target, $\dot{N}_1$, is given by

$$\dot{N}_1 = \frac{A_1 \cos \beta_1}{\pi \ell_1^2} N_o \ \text{sec}^{-1}. \tag{3}$$

The target is assumed to scatter the incident beam diffusely, so the molecular flux, $\dot{N}_2$, seen by a detector of area $A_2$, which is a distance $\ell_2$ from the target, and whose normal makes an angle $\beta_2$ with the target normal, is given[3] by

$$\dot{N}_2 = \frac{A_2 \cos \beta_2}{\pi \ell_2^2} N_1 \ \text{sec}^{-1}. \tag{4}$$

The molecular density, $n_2$, in the reflected beam at the detector[3] is

$$n_2 = \frac{\dot{N}_2}{A_2 \bar{v}_1} \text{ cm}^{-3}, \tag{5}$$

where $v_1 = (8kT_1/\pi m)^{1/2}$, and $T_1$ is the target temperature. By combining Eqs. 2-5, this density can be expressed as

$$n_2 = \frac{1}{4}\left(\frac{T_o}{T_1}\right)^{1/2} \frac{A_o \cos \beta_1}{\pi \ell_1^2} \frac{A_1 \cos \beta_2}{\pi \ell_2^2} n_o \text{cm}^{-3}. \tag{6}$$

The molecular flux $\dot{N}_o$ entering the chamber must be removed by the vacuum pumps, and thus has an upper limit that limits $n_2$, and hence the spectrometer signal.

A pump of speed S liters/sec removes gas from the vacuum chamber at a rate of $n_c S$ molecules/sec, where $n_c = P_c/kT_c$, $P_c$ and $T_c$ being the background pressure and wall temperature of the chamber. The steady-state condition is

$$\dot{N}_o = n_c S. \tag{7}$$

Combining Eqs. 2, 6, and 7 gives the beam density at the target

$$n_2 = S \frac{\cos \beta_1}{\pi \ell_1^2} \frac{\cos \beta_2}{\pi \ell_2^2} \frac{A_1}{\bar{v}_1} \frac{p_c}{kT_c}. \tag{8}$$

This determines the dependence of the signal magnitude on the chamber pressure, the pumping speed, and the dimensions of the molecular beam system.

b. Beam Modulation

The incident beam flux $\dot{N}_1$ is modulated by the chopper disc and, as a result, the scattered beam density $n_2$ is also modulated. If we neglect the velocity effects considered above, the functional form of $\dot{N}_1(t)$ is determined by the shape of the target, the chopping disc rotation frequency, f, and the geometry of the chopping disc. The form of $n_2(t)$ is determined by $\dot{N}_1(t)$ and the kinetics of the process occurring on the target, be it adsorption-desorption, adsorption-dissociation-desorption, adsorption-recombination-desorption, or adsorption-reaction with substrate-desorption. Since $n_2(t)$ is the quantity to be measured, it is necessary to know in what form it contains information on the surface process that is being investigated.

To calculate $\dot{N}_1(t)$, assume that the chopping disc is at a distance $\ell_o$ from the beam source, $A_o$ is very small relative to $A_1$, and $A_1$ is a rectangle of width $W_1$. The width of the beam, at the chopper disc, $W_o$, will be

$$W_o = \frac{\ell_o}{\ell_1} W_1. \tag{9}$$

If the chopper disc has a diameter d and n slits of width a, the beam $\dot{N}_1(t)$ will be characterized by three times:

(1) The chopping period, $t_o = \frac{1}{nf}$

(2) The "beam on" period, $t_p = \frac{a}{\pi d t_o}$

(3) The transition time, $t_1 = \frac{W_o}{\pi d} t_o$.

The function $\dot{N}_1(t)$ will be trapezoidal, and if j is an integer, we have

$$\dot{N}_1(t) = \dot{N}_1 \frac{t - jt_o}{t_1} \qquad 0 \leq t + jt_o \leq t_1 \tag{10a}$$

$$\dot{N}_1(t) = \dot{N}_1 \qquad t_1 \leq t + jt_o \leq t_p \tag{10b}$$

$$\dot{N}_1(t) = \dot{N}_1 \frac{t_1 + t_p - t + jt_o}{t_1} \qquad t_p \leq t + jt_o \leq t_p + t_1 \tag{10c}$$

$$\dot{N}_1(t) = 0 \qquad t_p + t_1 \leq t + jt_o \leq t_o \tag{10d}$$

If $W_o \ll a$, $\dot{N}_1(t)$ will be a rectangle characterized by $t_o$ and $t_p$, and the expression for the flux is

$$\dot{N}_1(t) = \dot{N}_1 \qquad 0 \leq t + jt_o \leq t_p \tag{11a}$$

$$\dot{N}_1(t) = 0 \qquad t_p \leq t + jt_o \leq t_o \tag{11b}$$

These two cases are shown in Figs. IX-3 and IX-4.

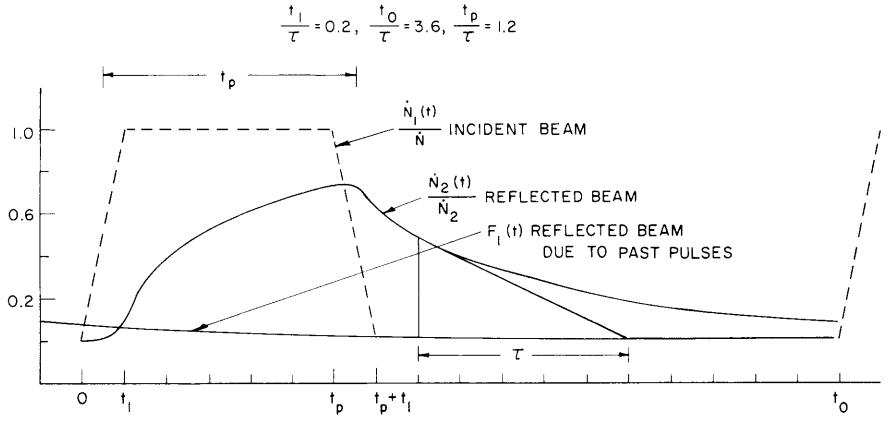


Fig. IX-3. Incident and reflected beam fluxes for a trapezoidal pulse.

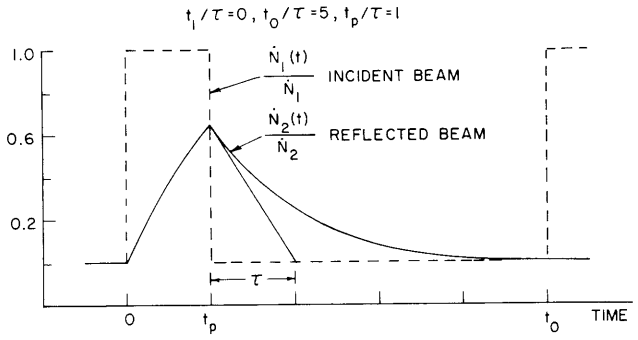


Fig. IX-4. Incident and reflected beam fluxes for a rectangular pulse.

Under the assumption that the probability that a beam particle arriving at the target at a time t' will either (a) desorb, (b) dissociate and desorb, (c) recombine and desorb, or (d) react and desorb at a time t is

$$P(t, t') = \frac{a}{\tau} e^{-(t-t')/\tau}, \tag{12}$$

the desorbed beam flux $\dot{N}_2(t)$ is given by

$$\dot{N}_2(t) = \frac{A_2 \cos \beta_2}{\pi \ell_2^2} \int_{-\infty}^{t} \dot{N}_1(t')\, P(t, t')\, dt'. \tag{13}$$

The number $a$ is the number of molecules created by one incident molecule during whatever process is taking place on the surface. For processes (a) and (d), $a = 1$; for process (b), $a = 2$; for process (c), $a = 1/2$. In the sequel, $a$ is assumed to be unity. Substituting Eqs. 10 and 12 in Eq. 13 and integrating gives

$$\dot{N}_2(t) = \dot{N}_2 \left[ \frac{t}{t_1} - \frac{\tau}{t_1}(1 - e^{-t/\tau}) + F_1(t) \right] \qquad 0 \leq t + jt_o \leq t_1 \tag{14a}$$

$$\dot{N}_2(t) = \dot{N}_2 \left[ 1 - e^{-t/\tau} \frac{\tau}{t_1} \left( e^{t_1/\tau} - 1 \right) + F_1(t) \right] \qquad t_1 \leq t + jt_o \leq t_p \tag{14b}$$

$$\dot{N}_2(t) = \dot{N}_2 \left[ \frac{t_1 + t_p - t}{t_1} + \frac{\tau}{t_1} \left( 1 + e^{-t/\tau} - e^{-(t-t_1)/\tau} - e^{-(t-t_p)/\tau} \right) + F_1(t) \right]$$

$$t_p \leq t + jt_o \leq t_p + t_1 \tag{14c}$$

$$\dot{N}_2(t) = \dot{N}_2 \left[ e^{-t/\tau} \left( e^{t_p/\tau} - 1 \right) \frac{\tau}{t_1} \left( e^{t_1/\tau} - 1 \right) + F_1(t) \right] \qquad t_p + t_1 \leq t + jt_o \leq t_o, \tag{14d}$$

where $F_1(t)$, the contribution to the desorbed beam flux from incident pulses arriving before $t + jt_o = 0$, is

$$F_1(t) = \frac{\tau}{t_1} e^{-t/\tau} \left(e^{t_p/\tau} - 1\right)\left(e^{t_1/\tau} - 1\right)\left(\frac{1}{e^{t_p/\tau} - 1}\right). \tag{15}$$

If $t_o/\tau \geq 5$, $F_1(t)$ can be neglected.

If $N_1(t)$ is given by Eqs. 11, integrating Eq. 13 gives for the desorbed beam flux

$$\dot{N}_2(t) = \dot{N}_2\left[1 - e^{-t/\tau} + F_o(t)\right] \qquad 0 \leq t + jt_o \leq t_p \tag{16a}$$

$$\dot{N}_2(t) = \dot{N}_2\left[e^{-t/\tau}\left(e^{t_p/\tau} - 1\right) + F_o(t)\right], \qquad t_p \leq t + jt_o \leq t_o, \tag{16b}$$

where $F_o(t)$, the contribution to the desorbed beam flux from incident pulses arriving before $t + jt_o = 0$, is

$$F_o(t) = e^{-t/\tau}\left(e^{t_o/\tau} - 1\right)\left(\frac{1}{e^{t_o/\tau} - 1}\right). \tag{17}$$

As with $F_1(t)$, $F_o(t)$ can be neglected when $t_o/\tau \geq 5$. Equations 14 and 16 are plotted in Figs. IX-3 and IX-4.

The experiment is designed to measure the quantity $\tau$, and Fig. IX-5 shows that $t_o$

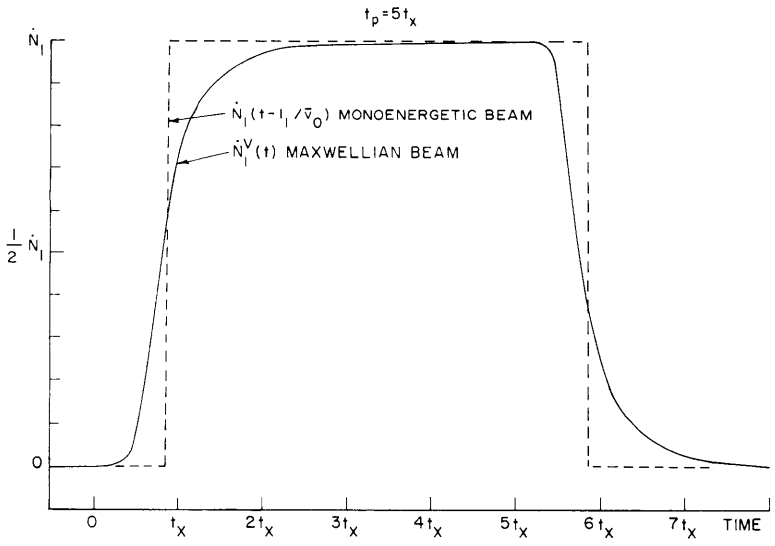


Fig. IX-5. Velocity spreading of incident beam.

must be equal to or a little greater than $5\tau$ to measure $\tau$ from the exponential tail of $n_2(t) = \dot{N}_2(t)/A_2\bar{v}_1$. The reason for this, as shown in Fig. IX-4, is that for $t_o < 5\tau$ the signal does not decay to less than 1% of $n_2$ when the next signal begins to arrive, and hence the zero level of the decay cannot be known. The frequency f must be adjusted to be equal to or a little less than the value

$$[f]_{max} = \frac{1}{5n\tau}. \tag{18}$$

This can be accomplished by observing that

$$\frac{\frac{d}{dt}[n_2(t)]\ t = \frac{2}{5}t_o}{\frac{d}{dt}[n_2(t)]\ t = \frac{3}{5}t_o} = e \tag{19}$$

is a consequence of Eq. 18.

c. Velocity Dispersion of the Beam

When the beam density $n_2(t)$ is a periodic signal with an exponential decay, the adsorption lifetime $\tau$ can be measured by the method discussed above. But under the assumption that the molecules in the beam have a Maxwellian distribution, the expressions $\dot{N}_1(t)$ and $\dot{n}_2(t)$ calculated above are valid approximations only for certain minimum values $t_o$ and $\tau$. These values must be calculated to eliminate the possibility of taking erroneous data.

If the gas in the source chamber is at equilibrium, the differential molecular flux can be written[4] as a function of velocity v as

$$P_3(Z)\,dZ = 4Z^3 e^{-Z^2}\,dZ, \tag{20}$$

where $Z = v/v_o$, and $v_o = (2kT_o/m)^{1/2}$. A molecule that leaves the chopper at a time t with velocity $v = Zv_o$ will arrive at $A_1$ at a time t, where

$$t' = t + \frac{\ell_1 - \ell_o}{v_o Z}. \tag{21}$$

If we define $t_x = (\ell_1 - \ell_o)/v_o$, the beam flux at the target will be

$$\dot{N}_1^v(t) = \int_0^\infty \dot{N}_1\left(t - \frac{t_x}{Z}\right) P_3(Z)\,dZ. \tag{22}$$

Using Eqs. 11 for $\dot{N}_1(t)$ and integrating gives

$$\dot{N}_1^v(t) = \dot{N}_1\left[1 + \left(\frac{t_x}{t}\right)^2\right] e^{-(t_x/t)^2} \qquad 0 \leq t \leq t_p \tag{23a}$$

$$\dot{N}_1^v(t) = \dot{N}_1\left\{\left[1 + \left(\frac{t_x}{t}\right)^2\right] e^{-(t_x/t)^2} - \left[1 + \left(\frac{t_x}{t - t_p}\right)^2\right] e^{-(t_o/t-t_p)^2}\right\} \qquad t_p \leq t \leq t_o. \tag{23b}$$

This is shown in Fig. IX-5 for $t_p = 5t_x$. Since most of the spreading of the rectangular pulse occurs over a time $t_x$, the condition

$$t_p \geq 10t_x \tag{24}$$

is arbitrarily imposed as a limit on $t_p$.

The differential molecular density[4] is

$$P_2(Z)\, dZ = \frac{4}{\sqrt{\pi}} Z^2 e^{-Z^2} dZ, \tag{25}$$

where here $Z = v/v_1$, and $v_1 = (2kT_1/\pi m)^{1/2}$. Defining $t_y = \ell_2/v_1$, a molecule leaving the target at time t' arrives at the detector at a time t, where

$$t = t' + \frac{t_y}{Z}. \tag{26}$$

The molecular density seen by the target is

$$N_2^v(t) = \frac{\cos\beta_2}{\pi\ell_2^2 v_1 \tau} \int_0^\infty \int_{-\infty}^{t-t_y/Z} \dot{N}_1^v(t')\, e^{-(t-t')/\tau}\, dt'\, P_2(Z)\, dZ. \tag{27}$$

This expression cannot be integrated analytically, so the conditions $t_p \geq 10\, t_x$ and $t_o \approx 5\tau$ are used to get a limit on $\tau$.

$$\tau \geq \frac{2t_o t_x}{t_p}. \tag{28}$$

The limitations on $\tau$ and $t_o$ will define a target temperature range over which data can be taken.

F. W. Eberle

## References

1. D. Steiner, "Orbital Electronegativity and Properties of Pure and Composite Metal Surfaces," Ph. D. Thesis, Department of Nuclear Engineering, M. I. T., 1967.
2. N. F. Ramsey, Molecular Beams (Oxford University Press, London and New York, 1956).

3. R. E. Stickney, "Atomic and Molecular Scattering from Solid Surfaces," in Advances in Atomic and Molecular Physics, Vol. III, edited by D. R. Bates and I. Estermann (Academic Press, Inc., New York, in press).

4. S. Yamamoto and R. E. Stickney, "Analysis of 'Lock-In' Detection of Modulated Molecular Beams Scattered from Solid Surfaces" (to appear in J. Chem. Phys.).

## B. SCREENING OF A POINT IMPURITY IN THE SURFACE REGION OF AN ELECTRON GAS

Recently, several investigations have been concerned with the surface properties of an electron gas. Interest is stimulated by the relevance of these studies to characteristic energy-loss experiments, in which surface, as well as volume, plasma modes are excited by fast incident electron beams, adsorption phenomena in which adsorbed ions polarize the inhomogeneous electron gas in the surface region, and bimetallic interface effects that require matching boundary conditions, thereby giving rise to observable properties.[1-6]

The present effort is concerned with the static screening of a point positive-charged impurity in the surface region of an electron gas. Expressions that will be justified formally in an article to be submitted for publication have been obtained[7] for the screening charge density as a function of position within the originally inhomogeneous electron gas. This many-body problem is fundamentally different from usual uniform electron gas problems, since the field penetration and hence screening occurs in that region of the electron gas in which the density is varying as a result of the surface boundary condition. The following formalism is based on the work of Baraff and Borowitz[8] and DuBois and Kivelson[9] for treating Thomas-Fermi atoms, Langer and Vosko[10] for impurity screening effects in uniform electron gases, Kohn and Sham[11] for treating general inhomogeneous electron gas effects, and some new ideas.[7]

Consider the many-electron system to be in a unit volume with an infinite repulsive barrier at the surface. Next, place a point impurity at the surface, which defines the origin of the coordinate system. The z-axis is perpendicular to the surface, and $\rho$ is the cylindrical radius in a plane parallel to the surface. With previous notation,[8,9] we can define single electron Green's functions in a mixed configuration and momentum space representation. To zero order in inhomogeneity corrections,

$$G_o(\underset{\sim}{R}, \underset{\sim}{p}) = \frac{1}{E - E(p) - \Sigma\,(\underset{\sim}{R}, \underset{\sim}{p}) - i\eta},$$

where the mass operator for the inhomogeneous system, according to Kohn and Sham, can be written as a sum of the local potential at a point $\underset{\sim}{R}$ plus a nonlocal short-range kernel. Fourier transforming their result with respect to relative electron coordinates

yields

$$\Sigma(\underset{\sim}{R}, \underset{\sim}{p}) = \phi(\underset{\sim}{R}) + \int d^3r\, M(\underset{\sim}{R}+\underset{\sim}{r}/2, \underset{\sim}{R}-\underset{\sim}{r}/2; E-\phi(\underset{\sim}{R}))\, e^{-i\underset{\sim}{p}\cdot\underset{\sim}{r}}, \tag{1}$$

where $\phi(\underset{\sim}{R})$ is the local potential, taken to be a screened Coulomb potential. The remaining term, which in a Hartree-like factorization of two-particle Green's functions is equal to zero,[7] is the short-range kernel.

The screening charge density is given by

$$\Delta n(\underset{\sim}{R}) = \frac{1}{2\pi i(2\pi)^3} \int_{p<p_F} d^3p\, dE\, \delta G_o(\underset{\sim}{R}, \underset{\sim}{p}). \tag{2}$$

If we consider electrons scattering through a single screened interaction from the impurity – a reasonable way of viewing the problem[10,11] – then use of the Kohn and Sham mass operator of Eq. 1 gives the Green's function correction

$$\delta G_o(\underset{\sim}{R}, \underset{\sim}{p}) \approx \int \frac{d^3p'}{E - E(p)}\, \phi(\underset{\sim}{R})\, \frac{1}{E - E(p')}\, \frac{\delta(\underset{\sim}{p}-\underset{\sim}{p}'-\underset{\sim}{q})}{(2\pi)^3}, \tag{3}$$

where q is the momentum transfer in the scattering event. The nonsymmetric screened interaction is written as a Fourier integral

$$\phi(\underset{\sim}{R}) = \int \frac{d^3q}{(2\pi)^3}\, \frac{v(q)}{\epsilon(q, o)}\, e^{i\underset{\sim}{q}_{||}\cdot\underset{\sim}{\rho}} \sin q_z z, \tag{4}$$

where $v(q) = (4\pi e^2)/q^2$, and $\epsilon(q, 0)$ is taken to be the RPA dielectric function. Heine[2] has suggested and Fedders[3] has proved the reasonability of using a spherically symmetric $\epsilon_{RPA}$ in the surface region when the surface barrier is infinitely repulsive. Use of Eqs. 3 and 4 in Eq. 2 gives

$$\Delta n(\underset{\sim}{R}) = \frac{1}{(2\pi)^3} \int_{\substack{|p+q|>p_F \\ p<p_F}} d^3p d^3q\, \frac{v(q)}{\epsilon(q, 0)}\, e^{i\underset{\sim}{q}_{||}\cdot\underset{\sim}{\rho}} \sin q_z z\, \frac{1}{\frac{p\cdot q}{m} + \frac{q^2}{2m}}.$$

The p integration is performed according to standard procedure. Hence

$$\Delta n(\underset{\sim}{R}) = \frac{1}{(2\pi)^3} \int d^3q \left(\frac{1}{\epsilon(q, 0)} - 1\right) e^{i\underset{\sim}{q}_{||}\cdot\underset{\sim}{\rho}} \sin q_z z, \tag{5}$$

which is the result obtained by Langer and Vosko[10] for a bulk impurity with the exception

of the sine factor replacing an exponential.

Through a procedure given elsewhere,[7] Eq. 5 can be reduced to a single integral on the magnitude of q. The result is

$$\Delta n(\underset{\sim}{R}) = \frac{p_F^3}{(2\pi)^2} \int_0^\infty dq \left( \frac{1}{\epsilon(q, 0)} - 1 \right) q \sin qz \frac{J_1(\rho q)}{\rho}, \tag{6}$$

which must be evaluated numerically.

As an example of the form of the results, Eq. 6 is evaluated for an electron gas at a density corresponding to $r_s = 3$ along the radial lines $\theta = 0°$, $30°$, and $60°$, where $\rho = R \sin \theta$ and $z = R \cos \theta$ and is shown in Fig. IX-6. These results are quite understandable. At $R = 0$ for any $\theta$, the initial charge density is zero, because of the infinite barrier.

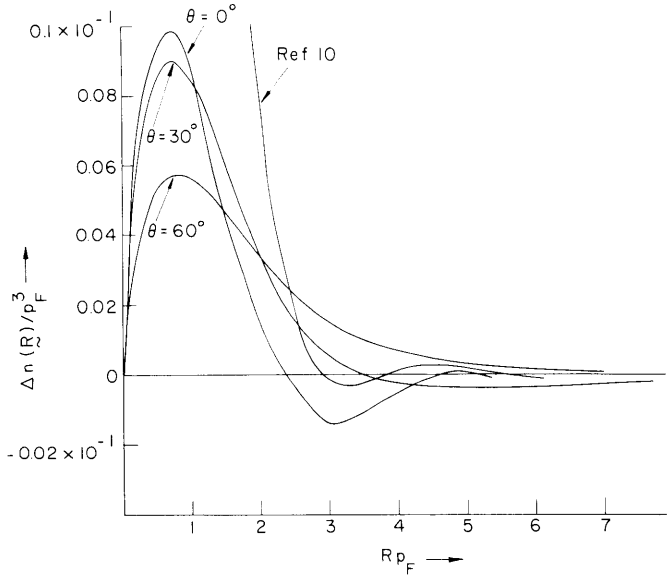


Fig. IX-6. Polarization charge density along the radial lines for $\theta = 0°$, $30°$, and $60°$, with $r_s = 3$. Also shown is the polarization charge density for an impurity in a uniform electron gas as derived by Langer and Vosko.[10]

Thus in the linearized model, there will be no polarization charge where initially there was no charge. As the weakly screened field penetrates into the gas, polarization charge builds up as the unperturbed electron density increases. Further into the electron gas past the point where the maximum screening charge density is seen, the screening becomes more effective and the polarization charge density decreases. For comparison,

the unperturbed electron gas density given by the expression

$$\frac{n_o(R)}{n_{internal}} = 1 - 3\left(\frac{\sin(2p_F R\cos\theta) - (2p_F R\cos\theta)\cos(2p_F R\cos\theta)}{(2p_F R\cos\theta)^3}\right)$$

is shown in Fig. IX-7. The unperturbed charge density builds up at a slower rate the larger $\theta$ is. For this reason, the long-range screening charge density for larger $\theta$ is greater, as is seen in Fig. IX-6.

A very significant feature of these results is the fact that the amplitude of the polarization charge density decays at a slower rate than the rate given by the customary expression $\delta n \approx (\cos 2p_F R)/R^3$ for describing Friedel oscillations around an impurity in the bulk metal. This is seen in Fig. IX-6 where the polarization charge density for a

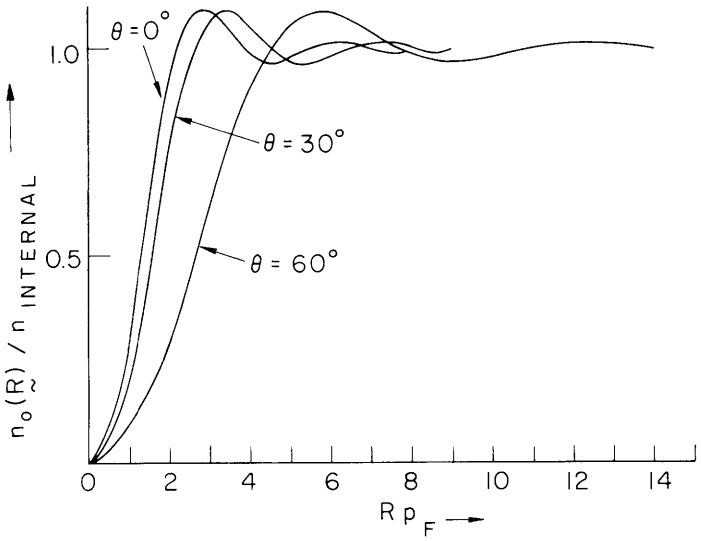


Fig. IX-7. Ratio of unperturbed charge density to interior density along the radial lines for $\theta = 0°$, 30°, and 60°, with $r_s = 3$.

bulk impurity, as obtained by Langer and Vosko, is also displayed. Since magnetic resonance and Knight shift experiments are often measuring effects occurring within the skin depth of metals, the conduction-band electron polarization around ion cores or impurities that are measured may display different long-range screening properties than those given by an $R^{-3}$ law. This surface screening effect should be taken into consideration before interpreting experimental data in terms of bulk theories. In the very distant oscillatory region, surface Friedel oscillations are superimposed on screening Friedel oscillations, thereby causing a complicated structured pattern of charge density.

The amplitude will decay at a rate within the range $R^{-3} < \delta n(\theta) < R^{-2}$, but the oscillatory behavior will not be as simple as a single trigonometric function. Because of this relatively long-range effect, measurable impurity-impurity interactions in dilute alloys may be greater than those inferred from bulk impurity theory.

It is also interesting to note the significance of these results for adsorption studies. A classical image force attraction to describe ion-metal interactions at short distances for which field penetration and bulk screening occur is frequently utilized.[12] In spite of this procedure, approximately good results obtain because the expectation value of the volume polarization charge calculated here is in approximately the same position relative to the surface as the commonly used image charge, a distance of the order of a few screening lengths. The long-range oscillating polarization charge gives only a negligible contribution to the net effect.

In a detailed article to be submitted for publication, formal justification and derivation of steps taken here will be given. Higher order inhomogeneity corrections in the schemes of Baraff[8] and DuBois[9] will be investigated. The short-range kernel reflecting inhomogeneity corrections will be dealt with beyond the Hartree approximation, extensive numerical results will be provided, and the use of these ideas for quantitatively understanding experimental situations will be presented.

J. W. Gadzuk

References

1. R. H. Ritchie and A. L. Marusak, Surface Sci. 4, 234 (1966).
2. V. Heine, Phys. Rev. 151, 561 (1966).
3. P. A. Fedders, Phys. Rev. 153, 438 (1967).
4. J. W. Gadzuk, Phys. Rev. 154, 622 (1967).
5. A. J. Bennett and C. B. Duke, Bull. Am. Phys. Soc. 11, 416 (1967).
6. F. Stern, Phys. Rev. Letters 18, 546 (1967).
7. J. W. Gadzuk, Quarterly Progress Report No. 64, Solid State and Molecular Theory Group, M. I. T., 1967.
8. G. A. Baraff and S. Borowitz, Phys. Rev. 121, 1704 (1961).
9. D. F. DuBois and M. G. Kivelson, Phys. Rev. 127, 1182 (1962).
10. J. Langer and S. J. Vosko, J. Phys. Chem. Solids 12, 196 (1960).
11. W. Kohn and L. J. Sham, Phys. Rev. 137, A1697 (1965); 145, 561 (1966), 150, 720 (1966).
12. J. W. Gadzuk, Surface Sci. 6, 133 (1967); 6, 159 (1967).

## C. CONTACT-POTENTIAL MEASUREMENTS OF THE ADSORPTION OF NITROGEN ON (110) TANTALUM

### 1. Introduction

The adsorption of nitrogen on tungsten has been widely studied by various techniques[1-7] and, although significant results have been obtained, the complexity of the process has hindered the development of a complete description. One interesting aspect of the problem has been the study of the relationship between surface structure and the change of work function which is due to $N_2$ adsorption. Contrary to expectations, $N_2$ adsorption upon some single-crystal surfaces of W produced decreases in the work function.[1] Since no data have been reported for $N_2$ on single-crystal tantalum, it seemed worth while for us to include $N_2$ in our general study of the contact-potential changes resulting from adsorption on (110) Ta. The results to be presented show qualitative, but not quantitative, agreement with (110) W results.

### 2. Apparatus

Since the apparatus has been described in detail previously,[8, 9] only the major features will be mentioned here. To avoid contamination by background gases, the apparatus was mounted within a large Varian ultrahigh vacuum system that maintained background pressures in the mid $10^{-11}$ Torr range during these runs.

The specimen studied was a Ta ribbon, $0.003 \times 0.127 \times 3.0$ cm, mounted upon a rotatable shaft. The ribbon was cut from a larger specimen which, when received, was reported to have a surface oriented in the (110) direction. The ribbon was analyzed by x-ray diffraction before use in the present studies, and gave a Laue pattern indicating a (110) orientation with noticeable lattice strain. The surface was cleaned by direct resistive heating to ~2500°K with occasional flashes to >2700°K.

Changes of work function caused by $N_2$ adsorption have been measured by the contact-potential method. For this measurement the target was positioned before a simple electron gun. To insure the constant emitter conditions required by the contact-potential method, the gun filament was continually run at ~2100°K. In addition to measuring changes in the surface work function, it was possible to measure the thermionic work function of the bare surface at a thermionic measurement station. Finally, a few runs were made in which the work function of the surface, with $N_2$ adsorbed, was measured photoelectrically.

A flask of $N_2$, connected to the system through a precise variable valve, was used to flood the system to a desired pressure. It was possible to obtain steady $N_2$ pressures ranging from $\sim 1 \times 10^{-9}$ Torr to $>10^{-6}$ Torr.

### 3. Experimental Method and Procedure

The theory, advantages and limitations of the contact-potential method have been described elsewhere[10,11] and will not be mentioned here. The method was implemented by the following procedure: Once a desired $N_2$ pressure had been established, the Ta surface was flash-cleaned and the work-function change monitored as a function of time.

In addition to $N_2$ adsorption runs, a few $N_2$ desorption runs were made. In these a certain nitrogen coverage was established and then the system was pumped back to the $10^{-11}$ Torr range. The surface was then flashed to some temperature for 15 sec and, upon cooling to 300°K, the work-function change (relative to the clean surface) was measured. The 15-sec flashes were continued by stepping the temperature to a higher value each time until the surface was apparently clean. These runs enabled us to estimate the desorption energy of $N_2$ on (110) Ta. It was not expected, however, that these runs would yield an entirely reliable value of desorption energy because significant desorption occurred in the low (1000°K-1500°K) temperature range where the temperature of the target was nonuniform.

### 4. Experimental Results

#### a. Thermionic Work Function

Measurements of thermionic emission from the target were used to calculate the effective work function.[11] A value of $\phi = 4.7 \pm 0.05$ eV was obtained for 4 measurements in the temperature range ~1750°K-~2300°K.

#### b. $N_2$ Adsorption on (110) Ta

In Fig. IX-8 the experimental results for $N_2$ adsorption on (110) Ta at 300°K are shown in terms of work-function change as a function of exposure to $N_2$. The exposure is defined simply as the product of the pressure and the time. In terms of the actual integrated particle flux, an exposure of $1 \times 10^{-9}$ Torr-minute, for example, is equal to $\sim 4.6 \times 10^{13}$ nitrogen atoms/cm$^2$.

Four general features are of interest in Fig. IX-8. First, over the entire exposure range that was studied, the work function change, caused by nitrogen adsorption, was always negative. Second, in the semilogarithmic plot of Fig. IX-8, the work function apparently decreases linearly with the log of the exposure (regardless of the pressure) up to a certain point. The third feature is that, for runs in the exposure range tested, the work function does not go through a minimum but rather reaches a plateau. The final feature is an apparent tendency for all runs, over the pressure range studied, to go to the same plateau value of work-function change. At the plateau the work-function change was -0.405 eV. The beginning of the plateau occurred at an exposure of $\sim 2 \times 10^{-6}$ Torr-minute. Although the runs span a pressure range of from $1 \times 10^{-9}$ Torr

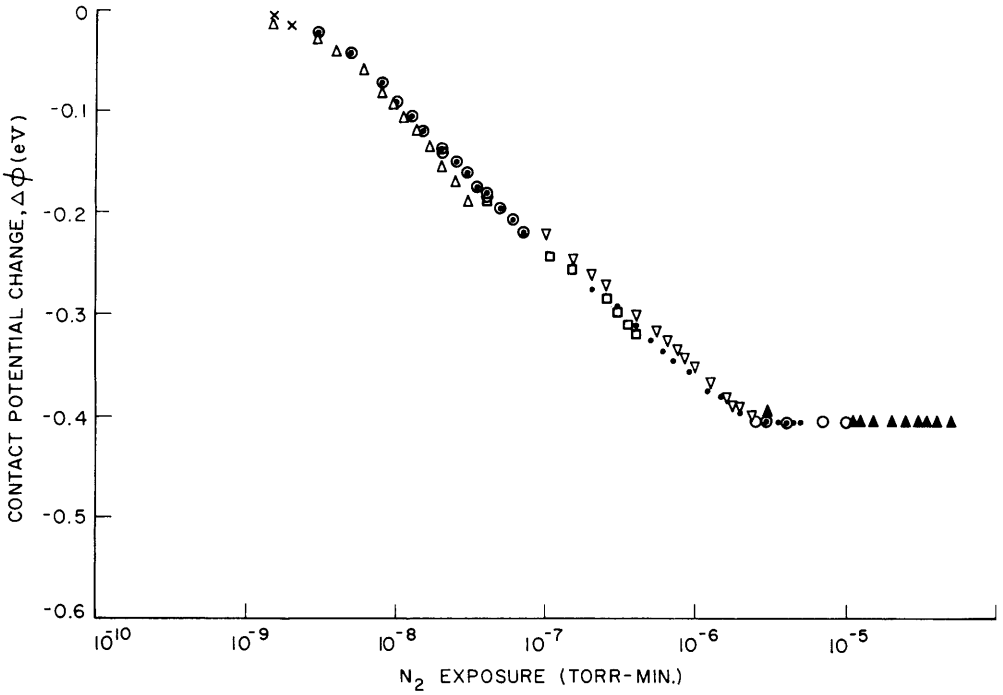


Fig. IX-8. Experimental results for $N_2$ adsorption on (110) Ta.

to ~$2 \times 10^{-6}$ Torr, it was not possible to reach the plateau region for the lower pressures without going to excessively long exposure times. Hence, points in the plateau region span only a pressure range from $5 \times 10^{-8}$ Torr to ~$2 \times 10^{-6}$ Torr. Once the plateau region had been reached, however, it was possible to decrease the pressure to $<10^{-9}$ Torr without seeing any further change in work function. If there were a pressure dependence at the power pressures we would have expected the magnitude of the work-function change to decrease when the pressure was suddenly decreased.

The results of two photoelectric runs were in qualitative agreement with the contact-potential results. In particular, these results indicated a shift in the photoelectric threshold to longer wavelengths with $N_2$ adsorption. This indicates a work function decrease due to $N_2$ adsorption, in agreement with the contact-potential results.

c. $N_2$ Desorption from (110) Ta

The data from two desorption runs were used to estimate desorption energies of $N_2$ from (110) Ta. Three major assumptions were used in making the calculation. First, it was assumed that nitrogen adsorbed dissociatively on the (110) Ta; second, that it desorbed as molecules. The third necessary assumption was that the work function change was directly proportional to the adsorbed nitrogen density. This convenient assumption is questionable. When this assumption is used, however, in conjunction

with the data of Fig. IX-8, it is possible to estimate $N_2$ sticking probabilities which appear reasonable when compared with sticking probabilities of $N_2$ on W.[7,12,13] The two values of desorption energy thus obtained were 0.71 eV (~16.5 kcal/mole) and 0.88 eV (~21 kcal/mole). No attempt was made to improve the accuracy of these measurements because a rough estimate of the desorption energy will be sufficient in the present study.

5. Discussion of Results

Since no data have been reported previously for $N_2$ adsorption on $T_a$, we shall make a qualitative comparison with existing data for W. The comparison will focus mainly upon the contact-potential study by Delchar and Ehrlich[1] of $N_2$ adsorption on several single-crystal faces of W. For (110) W it was found that when a work-function change occurred it was always negative; also, a very definite dependence of work-function change on pressure was also observed. For instance, at 300°K no adsorption occurred until the $N_2$ pressure was raised to ~$10^{-2}$ Torr. Also, the change of work function in the plateau region at this pressure was only -0.13 eV. If the target temperature were lowered to 110°K, adsorption occurred at $10^{-7}$ Torr and the maximum change in work function (at $10^{-6}$ Torr) was -0.15 eV. From the pressure dependence of the adsorption process, the estimated heat of adsorption was found to be $\leq$9 kcal/mole. Thus, although the magnitude of our work function change was considerably larger than that in Delchar and Ehrlich's (110) W study, a decrease was seen in both cases. The negative change in work function has also been seen by several other researchers for nitrogen adsorption on various tungsten samples.[2-6] Since possible reasons for such decreases have been discussed elsewhere, they will be omitted here.

The interesting difference between our data and the (110) W data is in the apparent lack of pressure dependence in the case of $N_2$ on (110) Ta. As confirmed by our estimate of the desorption energy, our data are indicative of a desorption energy appreciably higher than that for (110) W. The existence of the sharp plateau is also interesting. If we assume that the adsorption of $N_2$ will always produce a corresponding change in work function, then the existence of the plateau indicates that no further adsorption occurs beyond an exposure of ~$2 \times 10^{-6}$ Torr-minute. This, in turn, indicates a saturation of the surface adsorption sites, with a binding energy for $N_2$ appreciably greater than 9 kcal/mole. Finally, the data are also consistent with the assumption that nitrogen adsorption occurs by dissociation into atoms, and that desorption occurs by the formation of $N_2$ molecules. The data are not consistent with the assumption that both adsorption and desorption occur as molecules; for, when this assumption is used in estimating desorption energies from the desorption data, the values obtained are significantly lower than those obtained under the first assumption. Based on the energies thus obtained, we would expect to see a significant pressure effect in our data if the

second assumption were correct. Since this was not seen, this assumption is not consistent with our results.

D. L. Fehrs

References


1. T. A. Delchar and G. Ehrlich, J. Chem. Phys. 42, 2686 (1965).
2. G. Ehrlich and F. G. Hudda, J. Chem. Phys. 35, 1421 (1961).
3. M. P. Hill and B. A. Pethica, J. Chem. Phys. 36, 3095 (1962); 38, 567 (1963).
4. F. W. Hayes, M. P. Hill, S. M. A. Lecchini, and B. A. Pethica, J. Chem. Phys. 42, 2919 (1964).
5. T. Oguri, J. Phys. Soc. Japan 19, 83 (1964).
6. A. A. Holscher, J. Chem. Phys. 41, 579 (1964).
7. M. P. Hill, S. M. A. Lecchini, and B. A. Pethica, J. Chem. Phys. 44, 2170 (1966).
8. D. L. Fehrs and R. E. Stickney, Quarterly Progress Report No. 82, Research Laboratory of Electronics, M.I.T., July 16, 1966, p. 77.
9. D. L. Fehrs and R. E. Stickney, Quarterly Progress Report No. 84, Research Laboratory of Electronics, M.I.T., January 15, 1967, pp. 82-89.
10. P. A. Anderson, Phys. Rev. 47, 958 (1935).
11. W. B. Nottingham, "Thermionic Emission," Technical Report 321, Research Laboratory of Electronics, M.I.T., December 10, 1956.
12. G. Ehrlich, J. Chem. Phys. 34, 29 (1961).
13. F. M. Wanlass and H. Eyring, Solid Surfaces and the Gas Solid Interface (American Chemical Society Publications, Washington, D.C., 1961), p. 140.


## D. THERMIONIC AND ADSORPTION PROPERTIES OF POLYCRYSTALLINE REFRACTORY METALS EXPOSED TO OXYGEN

### 1. Introduction

Some interest has been shown recently in the enhancement of thermionic emission from cesium-covered surfaces by the introduction of controlled amounts of oxygen. This is relevant to the operation of thermionic energy converters.[1]

This study is aimed at obtaining the effects of adsorbed oxygen on the thermionic properties of the materials most commonly used as emitters in thermionic diodes, that is, the refractory metals, tungsten, molybdenum, tantalum, and rhenium.

Earlier experiments of the type described below were performed by Engelmaier on single-crystal tungsten.[2,3]

### 2. Apparatus

The apparatus comprised an accurately measured, polycrystalline filament of the particular material, suspended in a cylindrical collector-guard-ring structure mounted

in a high-vacuum system. Two identical assemblies were placed symmetrically about the pumping ports to enable comparison of the behavior of the molybdenum, tantalum, and rhenium filaments in turn with the same tungsten filament in precisely the same atmosphere.

The vacuum system consisted of two series-connected Mercury diffusion pumps in parallel with a cryopump containing liquid helium or liquid nitrogen. Various pressures of oxygen were established by opening a finely controlled motor-driven Granville-Phillips valve between the system and a bottle of high-purity laboratory oxygen. The pressures were monitored by using a General Electric ionization gauge (Model 22GT102) on each tube. These gauges measure equivalent nitrogen pressure and were always used on the thoriated iridium filament that operates at a lower temperature than one of pure tungsten, and hence fewer errors attributable to interactions with the hot filament result.

3. Procedure

Two kinds of tests were performed. First, saturation current measurements were taken at various oxygen pressures and filament temperatures. Second, rates of oxygen desorption were obtained at various filament temperatures by introducing oxygen to a pressure of $6 \times 10^{-5}$ mm Hg with the filament cold (1400°K), and then either raising the filament to the desired temperature and then quickly pumping out by using the cryopump, as well as the diffusion pumps, or pumping out first and then quickly flashing the filament to the required temperature. Both of these methods have been used in previous desorption studies,[3,4] and comparison between the two was desirable.

Furthermore, the oxygen was adsorbed at different temperatures before runs at the same desorption temperature to try to observe any differences that this may produce in the desorption energy.

a. Calculation of Parameters from Experimental Results

Effective work functions ($\Phi$) in eV are obtained from the following form of the Richardson equation:

$$J = 120\, T^2 \exp\left(\frac{-e\Phi}{kT}\right) \text{ amps/cm}^2,$$

where J is saturated current density, T is filament temperature, and k is Boltzmann's constant.

Desorption energies are calculated under the following assumptions.

(i) Desorption is a first-order process; that is, $\theta = \theta_i \exp\left(\frac{-t}{\tau}\right)$, where $\theta$ = coverage at a time t sec after the coverage was $\theta_i$; and $\tau$ is the characteristic adsorption time at a particular temperature and coverage.

(ii) In the range of coverage considered, $\Phi \propto \theta$.

(iii) The relationship between $\tau$ and the desorption energy E is given by

$$\tau = \tau_o \exp\left(\frac{eE}{kT}\right),$$

where E is in eV, and $\tau_o$ is a constant of the order of the time period of vibration of an atom in the metal lattice.[4]

From assumptions (i) and (ii) and their connected equations, the following relationship can be derived.[3]

$$\tau = (t_I - t)\left[\log_e\left(\frac{\log_e I_o/I}{\log_e I_o/I_I}\right)\right]^{-1},$$

where $I_o$, I, $I_I$, are the saturated currents at zero oxygen coverage, time t, and time $t_I$, respectively.

E can be determined at various times during the desorption run and related to a parameter $\theta^* = \Phi - \Phi_o$ (which at low coverage is directly proportional to $\theta$), where $\Phi_o$ is the "bare" work function, and $\Phi$ is the mean work function over the period of time used to calculate $\tau$.

E is obtained by either assuming a value of $\tau_o = 1 \times 10^{-13}$ sec or by a plot of $\log_e \tau$ against $\frac{1}{T}$, which yields slope E and intercept $\log_e \tau_o$.

The parameter $T/T_R^*$ has proved useful in other studies for correlating $\Phi$ for various temperatures and pressures, where $T_R^*$ is the "effective reservoir temperature" required to establish a certain oxygen pressure. Pressure and $T_R^*$ are related by[2,3]

$$\log_{10} p = 9.25 - \frac{486.45}{T_R^*} \text{ for oxygen.}$$

4. Results

The experimental data are shown in Figs. IX-9 through IX-15.

Reliable results for tantalum were not obtained because of the great difficulty of experimenting with this material. Those results that were obtained were unreproducible, as they depended greatly on the complete past history of the filament. After the first run in oxygen, it proved impossible to regain the initial bare-work-function state, even allowing for the recalibration of temperature that was noted as necessary by Langmuir and Malter.[5] Furthermore, the work function showed a temporal variation even under identical conditions, thereby indicating that perhaps tantalum exhibits marked absorption, as well as adsorption, effects.

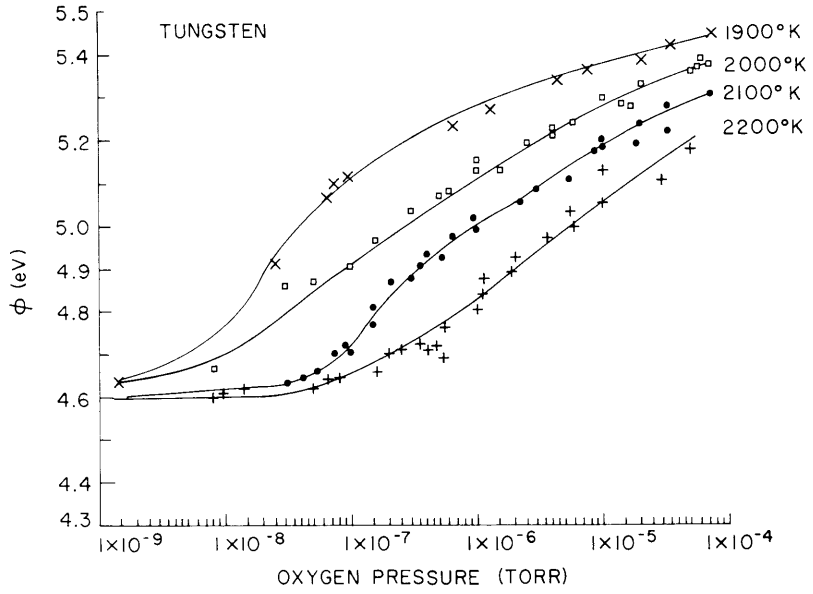


Fig. IX-9. Work function vs $\log_{10}$ (pressure) for tungsten.

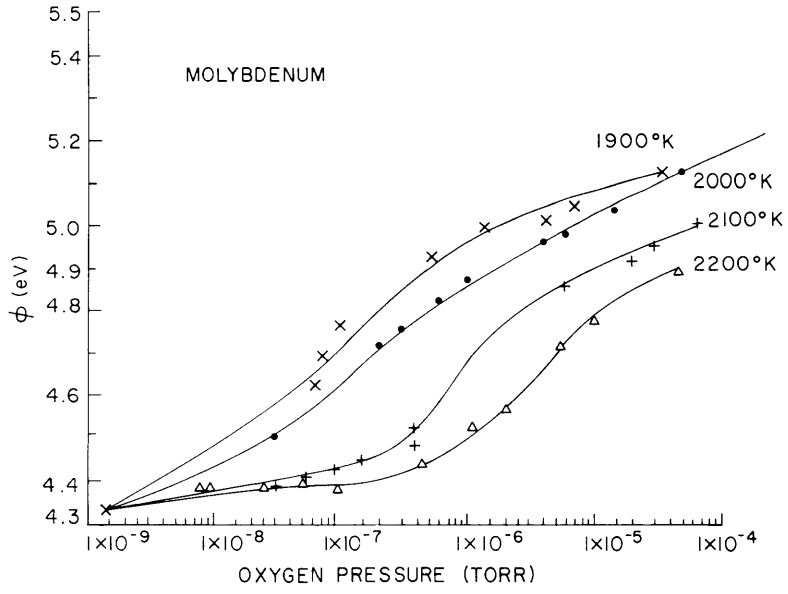


Fig. IX-10. Work function vs $\log_{10}$ (pressure) for molybdenum.

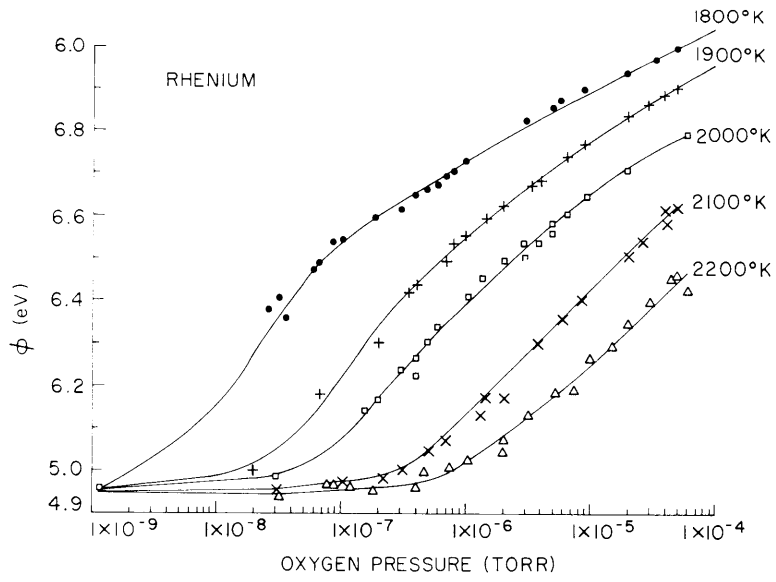


Fig. IX-11. Work function vs $\log_{10}$ (pressure) for rhenium.

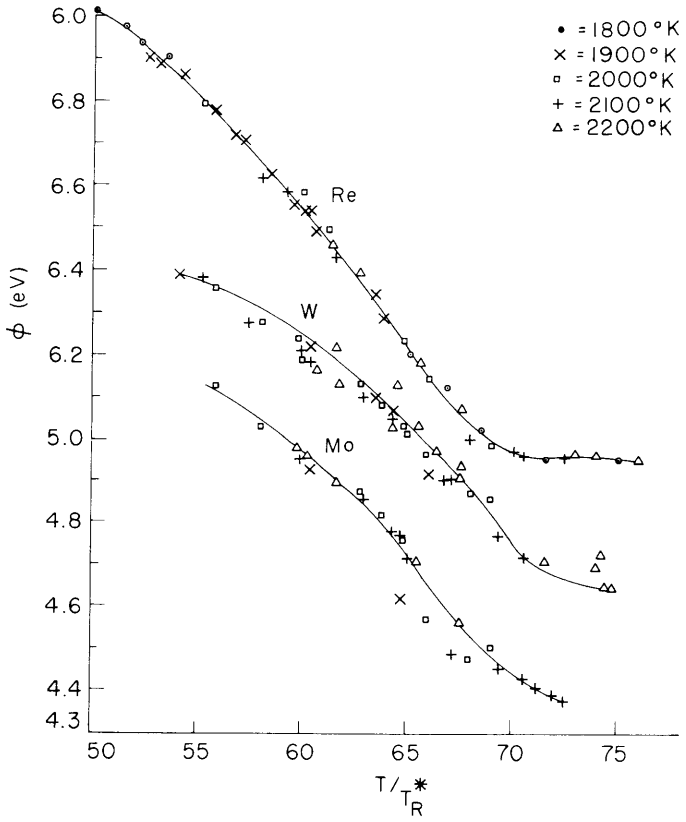


Fig. IX-12. Work function vs $T/T_R^*$.

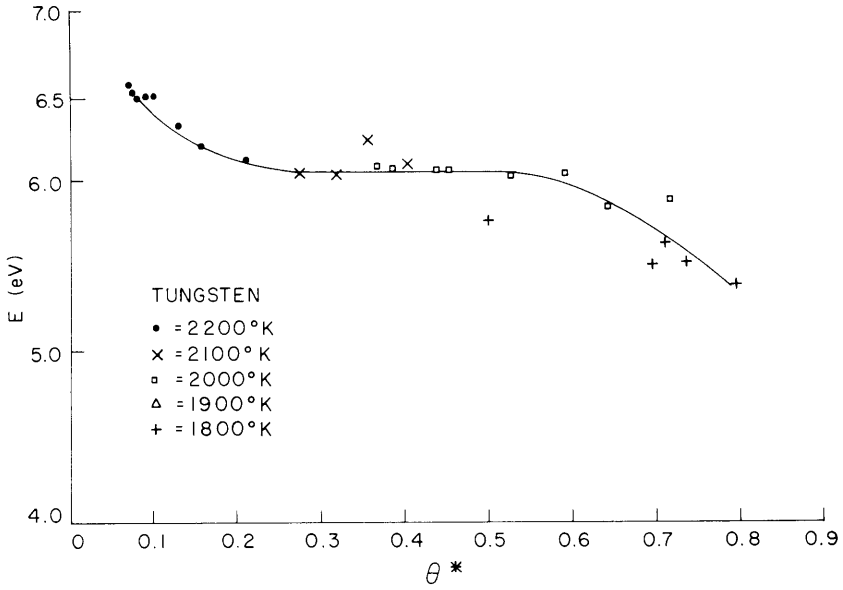


Fig. IX-13. Desorption energy vs $\theta^*$ for tungsten.

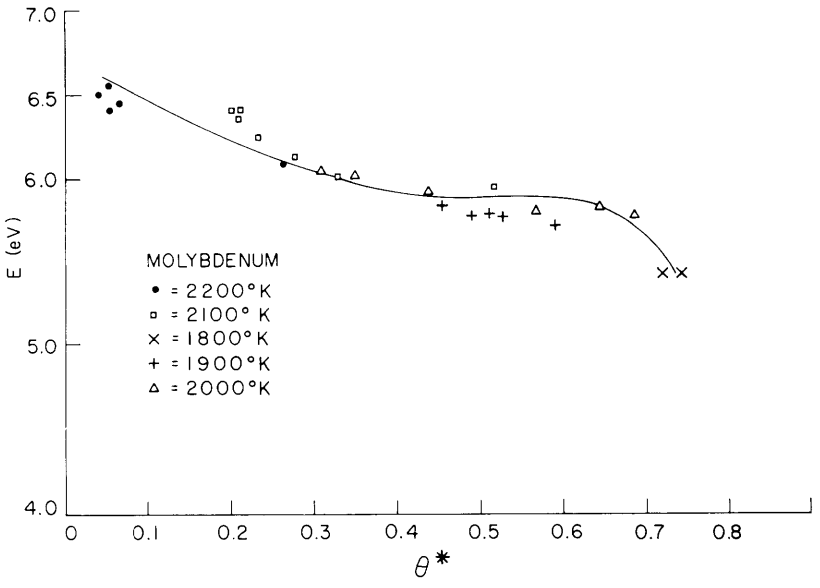


Fig. IX-14. Desorption energy vs $\theta^*$ for molybdenum.

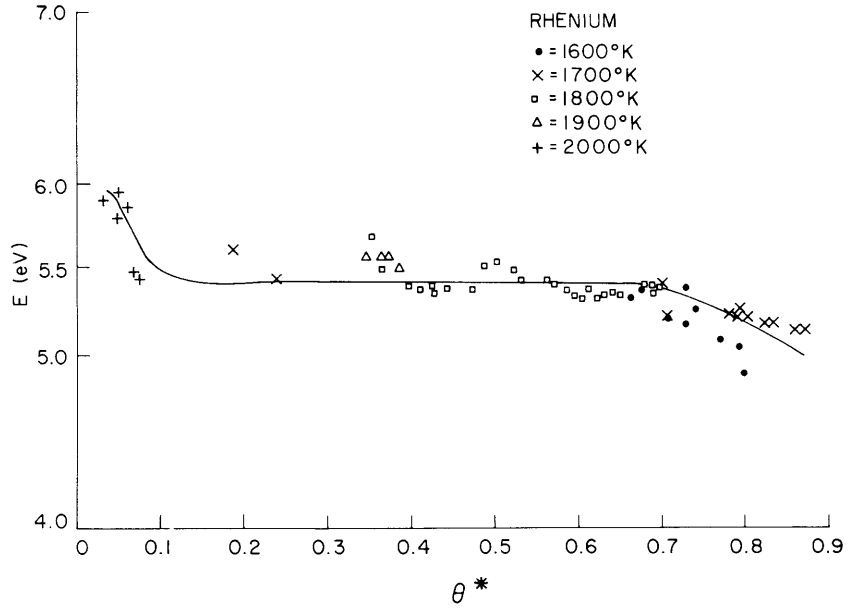


Fig. IX-15. Desorption energy vs $\theta^*$ for rhenium.

5. Discussion

a. Desorption Measurements

The plot of E against $\theta^*$ indicates that E apparently rises at the lower coverages and falls at the higher coverages and is constant over the intermediate range. The increase at the lower values is probably not a genuine property of the material, but may rather be due to the oxygen slowly desorbing from the tube walls and collector and creating a finite background oxygen pressure that partially compensates for further desorption from the filament. The decrease at higher values is probably a genuine effect. The constant value attained in the tungsten plot in the intermediate range corresponds very closely to that obtained by Engelmaier and Stickney[3] in single-crystal tungsten experiments. This result suggests that some migration of oxygen atoms on the surface occurs at a rate that is fast compared with the rate of desorption. It should be noted that, with this variation of E, comparison of values of E determined by experiment should be quoted for particular values of coverage. (Cf. values given by Johnson and Vick[4] for oxygen desorption from polycrystalline tungsten which were obtained at low coverages.)

Attempts to determine E from log $\tau$ vs $1/T$ did not succeed, because of the experimental scatter of values of $\tau$, so that all values of E were determined by assuming $\tau_o = 1 \times 10^{-13}$ sec.

Within the experimental limits there appeared to be no difference between values

of E obtained with the different experimental techniques and the different temperatures at which the oxygen was adsorbed.

b. Work Function/Pressure Measurements

The work function/pressure curves for the different materials show the same qualitative behavior. In all cases, the effective work function of the bare surface is not the same for different temperatures, and the maximum work-function change is not produced in the range of pressures that was used.

The use of the parameter $T/T_R^*$ to correlate values of $\Phi$ from different temperature runs proved satisfactory, particularly for rhenium. The small amount of scatter is probably due to slight (0.5 per cent) inaccuracies in the temperature setting between runs.

6. Conclusions

The values of desorption energy listed in Table IX-1 are calculated under the assumption that $\tau_o = 1 \times 10^{-13}$.

Table IX-1. Values of desorption energy.

| Material | Range of $\theta^*$ | E (eV) | Tolerances (eV) | Approximate Adsorption Energies[6] (eV) |
|---|---|---|---|---|
| Tungsten | 0.3 to 0.6 | 6.05 | ±.05 | 8.3 |
| Molybdenum | 0.4 to 0.6 | 5.9 | ±.1 | 7.5 |
| Rhenium | 0.3 to 0.7 | 5.40 | ±.05 | 6.5 |

Note: The value of adsorption energies for rhenium is found by assuming that rhenium fits into the pattern of variation of adsorption energy with atomic radius given by Brennan, Hayward and Trapnell.[6]

W. Greaves

References

1. D. Lieb and S. Kitrilakis, Thermionic Conversion Specialist Conference, Houston, Texas, 1966.
2. W. Engelmaier and R. Stickney, Quarterly Progress Report No. 82, Research Laboratory of Electronics, M.I.T., July 15, 1966, p. 71.
3. W. Engelmaier and R. E. Stickney, Report on Twenty-sixth Annual Conference on Physical Electronics, M.I.T., Cambridge, Mass., March 21-23, 1966, p. 260.
4. M. Johnson and F. Vick, Proc. Royal Soc. (London) A151, 296 (1935).
5. L. Malter and D. B. Langmuir, Phys. Rev. 55, 743 (1939).
6. D. Brennan, D. Hayward, and B. Trapnell, Proc. Royal Soc. (London) A256, 81 (1960).